Vol. 499: 47–64, 2014
doi: 10.3354/meps10630

MARINE ECOLOGY PROGRESS SERIES
Mar Ecol Prog Ser

Published March 3

Effects of community composition and size structure on light absorption and nutrient uptake of phytoplankton in contrasting areas of the Alboran Sea

Jesús M. Mercado[1,*], Iria Sala[1], Soluna Salles[1], Dolores Cortés[1], Teodoro Ramírez[1], Esperanza Liger[2], Lidia Yebra[1], Begoña Bautista[3]

[1]Centro Oceanográfico de Málaga, Instituto Español de Oceanografía, 29640 Fuengirola, Málaga, Spain
[2]Departamento de Física Aplicada II, University of Málaga, 29070 Málaga, Spain
[3]Departamento de Ecología y Geología, University of Málaga, 29070 Málaga, Spain

ABSTRACT: Biomass size distribution, light absorption properties and carbon and nitrogen uptake rates were analysed in phytoplankton assemblages along coast–offshore gradients. During sampling, the coastal stations were affected by upwelling. In contrast, the offshore stations were located at the western Alboran anticyclonic gyre core. Surface nitrate concentration was >1 µM at the coastal stations and lower than the detection limit at the offshore stations. Furthermore, the lower limit of the upper mixed layer was deeper at the coast (ca. 20–30 m depth) than offshore (80–100 m depth). In terms of biomass, the coastal communities were dominated by diatoms; dinoflagellates and picoplankton contributed to phytoplankton biomass by <30 and 7%, respectively. At the offshore stations, diatom abundance decreased while dinoflagellate abundance did not change significantly in comparison to the coastal stations, with dinoflagellates becoming the dominant group in terms of biomass. The mean length of the microplankton cells increased from the coast to offshore due to a decrease in abundance of diatoms <50 µm in length. The coastal communities featured lower chl *a* specific absorption coefficients in the blue spectral band than found in the offshore communities. In contrast, the biomass-specific uptake rates of inorganic carbon and nitrate estimated for the coastal communities (3.5 nmol C μg^{-1} POC h^{-1} and 0.2 nmol N μg^{-1} POC h^{-1}, respectively) were higher than for the offshore communities (1.0 nmol C μg^{-1} POC h^{-1} and 0.03 nmol N μg^{-1} POC h^{-1}, respectively). These differences in light absorption efficiency and nutrient uptake rates were significantly correlated with the change in the mean cell size of the communities moving from the coast to offshore, which were mainly due to the decrease in biomass of diatoms <50 µm which effectively increased the dinoflagellate contribution to phytoplankton biomass.

KEY WORDS: Anticyclonic gyre · Primary productivity · Diatoms · Upwelling · Carbon uptake · Nutrients

INTRODUCTION

Cell size modulates light absorption and nutrient uptake by phytoplankton. Theoretically, the probability of absorbing photons per chlorophyll unit under a given light field decreases with increasing cell size; consequently, the efficiency of light absorption in large cells should be reduced in comparison with small cells (Geider et al. 1986, Raven & Kübler 2002). Laboratory data obtained from experiments performed with isolated cultures corroborate this expected relationship between cell size and light absorption properties (e.g. see Finkel 2001). Coincidently, phytoplankton communities dominated by small cells

*Corresponding author: jesus.mercado@ma.ieo.es

(cell size < 2 µm) feature higher values of light absorption coefficient per chl *a* unit than communities dominated by larger phytoplankton (Ciotti et al. 2002, Ciotti & Bricaud 2006). Ciotti et al. (2002) concluded that about 80% of variability in the absorption properties of the phytoplankton can be explained by changes in the mean size of the communities. On the other hand, small cells theoretically require lower nutrient concentrations than large cells to keep an equivalent influx per volume unit (Armbrust & Chisholm 1992). As a result, small cells should maintain high growth rates at low nutrient concentrations, while large cells have a higher capacity for nutrient uptake at high nutrient concentrations. Recently, Edwards et al. (2012) reviewed the relationship between nitrate and phosphate uptake kinetic parameters per cell and cell size in phytoplankton. According to that study, both nutrient uptake maximum rate per cell and half-saturation constant tend to increase with cell volume. Concordantly, field data indicate that nitrate uptake rates are normally higher for large-sized phytoplankton than for small-sized cells (Harrison & Wood 1988, Tremblay et al. 1997).

Based on these relationships between resource acquisition and cell size, size constraints have been used to explain the main macro-ecological distribution patterns of phytoplankton. Thus, it has been postulated that the predominance of communities dominated by large cells in upwelling or high dynamic areas (i.e. under non-restrictive conditions of nutrients or light, at least temporally) is related to their higher growth rates and carbon-specific photosynthesis in comparison with small phytoplankton (Stolte & Riegman 1995, Raven & Kübler 2002, Lohrenz et al. 2003, Irwin et al. 2006, Litchman et al. 2009, Key et al. 2010). In contrast, dominance of picoplankton in poor nutrient and strong stratified open ocean waters is normally attributed to a higher affinity of this group for nutrients (Agawin et al. 2002, Gutiérrez-Rodríguez et al. 2011, Silovic et al. 2011). However, exceptions to this expected relationship between nutrient usage and community size structure have been described (Rodríguez et al. 2001, Armstrong 2003, Morin & Fox 2004, Nogueira et al. 2004, Irigoien et al. 2005). Normally, these deviations are attributed to biological interactions (e.g. grazing) that could have a preponderant role in regulating the abundance of some size groups in several ecosystems.

The aim of this study was to assess if shifts in taxonomic composition and biomass size distribution of phytoplankton communities in the Alboran Sea are reflected in their light absorption efficiencies and nutrient uptake rates according to the expected theoretical relationships between size constraints and metabolism. This hypothesis was tested by analysing the results of an oceanographic research survey conducted in contrasting areas (coastal upwelling vs. offshore oligotrophic areas) of the western Alboran Sea. The jet of Atlantic water that penetrates into the Alboran Sea through the Strait of Gibraltar feeds 2 nutrient depleted quasi-permanent anticyclonic gyres which occupy the entire central part of the western and eastern sub-basins (Parrilla & Kinder 1987, Minas et al. 1991, Tintoré et al. 1991). At the northern edge of the western anticyclonic gyre there are intense geostrophic fronts that promote upwelling of subsurface waters. Furthermore, the upwellings are frequently intensified by favourable winds blowing along the northern coast (Parrilla & Kinder 1987, Sarhan et al. 2000). Consequently, the presence of strong decreasing gradients of nutrients and chlorophyll from the coast to offshore is a typical feature of the northwestern Alboran Sea (Rodríguez 1994, Ramírez et al. 2005, Mercado et al. 2007, 2012). The changes in the shape of the phytoplankton size spectra in this Alboran sub-basin have been extensively studied (Rodríguez et al. 2001, Arín et al. 2002, Reul et al. 2005). There is also available information about light absorption properties and nutrient uptake kinetics (Arín et al. 2002, Mercado et al. 2008a). However, studies analysing the relationship between size structure and metabolism are scarce.

MATERIALS AND METHODS

Sampling was carried out in the northwest Alboran Sea (latitude 35° 54′–36° 33′ N and longitude 4° 11′–4° 54′ W) between 9 and 14 May 2008, on board RV 'García del Cid' in the framework of Project NITROALBORAN. Ten stations distributed along 2 transects perpendicular to the coast were sampled (Fig. 1). A vertical profile of temperature, salinity and chl *a* fluorescence was obtained at each station with a CTD Seabird 25 equipped with a fluorescence probe (Seapoint 6000) and a photosynthetically active radiation (PAR) radiometer (LICOR). The euphotic layer depth at each station was estimated from the ascending profiles of PAR to be the depth at which 1% of surface irradiance was reached. The mixed-layer (ML) depth was estimated in accorcance with the method proposed by Kara et al. (2000) based on the use of a finite difference criterion, where the ML depth is the depth at which potential density has changed by a fixed amount from the surface reference value. Specifically, the ML depth was estimated as that at

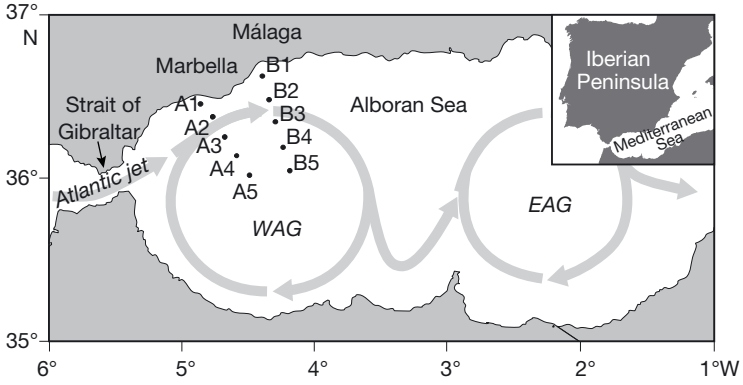

Fig. 1. Position of the sampling stations along 2 transects perpendicular to the coast. Grey arrows indicate the surface circulation pattern characteristic of the Alboran Sea. It is representative of the hydrological dynamics that occurred during the sampling cruise (WAG, western anticyclonic gyre; EAG, eastern anticyclonic gyre)

which the density difference from the surface was 0.5. This threshold was chosen because in previous studies performed in the northern Alboran Sea (Mercado et al. 2007, 2008a,b) it gave the highest success rate for finding the proper pycnocline. Additionally, vertical variation in the Brunt-Väisälä frequency (N^2) was estimated at each station from the potential density profiles in accordance with Millard et al. (1990).

Samples of seawater were collected with a rosette equipped with Niskin bottles at 7 fixed depths (0, 10, 20, 30, 50, 75 and 100 m). An additional sample was collected at the depth where the subsurface chl *a* fluorescence maximum (SFM) was detected (usually between 20 and 50 m depth). For nutrient analyses, 2 replicates of seawater from each of the 7 depths were taken and immediately frozen at −20°C. In the laboratory, nutrients (nitrate plus nitrite, nitrite, ammonium, phosphate and silicate) were analysed by means of segmented flow analysis using a Bran-Luebbe AA3 autoanalyser, following the methods described in Ramírez et al. (2005). The detection limits were 0.05 µM for nitrate, 0.01 µM for nitrite, 0.04 µM for phosphate and ammonium and 0.10 µM for silicate. For the determination of chl *a*, 0.5 to 1 l of seawater was filtered through Whatman GF/F filters which were subsequently frozen at −20°C until their analysis in the laboratory. The analysis of chl *a* was conducted by spectrophotometry, after extraction in 90% acetone overnight at 4 to 5°C.

Structure of the phytoplankton communities

Abundances of *Prochlorococcus*, *Synechococcus*, eukaryotic picoplankton and nanoplankton were determined in samples collected at each of the 7 depths. The samples were fixed with glutaraldehyde (1% final concentration) and immediately frozen in liquid nitrogen (Vaulot et al. 1989). The samples were analysed with a Becton Dickinson FACScan flow cytometer. Counting of cells was performed based on the forward-light scatter and the orange and red fluorescence signals. BD TrueCOUNT Tubes were used to determine absolute counts. Abundance and taxonomy of phytoplankton >5 µm were determined in water samples collected at the surface and SFM depth. The water samples were fixed in dark glass bottles with Lugol's solution (2% final concentration). In the laboratory, 100 ml of each fixed sample were sedimented in a composite chamber for 24 h, following the technique developed by Utermöhl (1958). Cells were counted at 200× and 400× magnification with a Leica DMIL inverted microscope connected to a Leica DFC video-camera. The species nomenclature was validated using Tomas (1997).

Cell biovolume of the most abundant species and genus of diatoms and dinoflagellates was calculated by using the most appropriate formula according to their geometric shape (Sun & Liu 2003, Olenina et al. 2006, Vadrucci et al. 2007). Biovolume of unidentified autotrophic flagellates was also calculated. The values of cell axis length measured by image analysis with Leica Application Suite software were used to perform these calculations. Equivalent spherical diameter (ESD) of each cell was estimated from the length of the longer axis. Biovolume of 42 taxonomic groups (most of them genera or species of diatoms) were characterised. Biovolumes of *Synechococcus*, *Prochlorococcus*, nanoeukaryotes and picoeukaryotes were calculated using the values given in Ribes et al. (1999) for samples collected in the northwestern Mediterranean Sea. Biovolume values were converted into biomass using the formulae proposed by Morel et al. (1993) for *Prochlorococcus*, Kana & Glibert (1987) for *Synechococcus*, Verity et al. (1992) for phytoplankton <15 µm in length and Menden-Deuer & Lessard (2000) for dinoflagellates and diatoms >15 µm in length.

Light absorption properties

Absorption spectra were obtained on Whatman GF/F filters with a Shimadzu UV10100 spectrophotometer following the modified method by Trüper &

Yentsch (1967). The absorbance of the filters (OD_{filt}) before and after the extraction of the chl *a* with acetone was measured as described in Mercado et al. (2008b). The equation proposed by Cleveland & Weidemann (1993) was used to calculate the absorbance spectrum of the suspension, $OD_{susp}(\lambda)$, from $OD_{filt}(\lambda)$. The absorption coefficient, $a(\lambda)$, was calculated according to:

$$a(\lambda) = 2.3\ OD_{susp}(\lambda) / (V/A) \quad (1)$$

where V is the filtered volume (m^3) and A is the filtered area (m^2).

The absorption coefficient of the phytoplankton, $a_{phy}(\lambda)$ (m^{-1}), was calculated by subtracting the absorption of particulate matter, $a_p(\lambda)$ (m^{-1}), from detritus, $a_d(\lambda)$ (m^{-1}), which were obtained before and after extraction, respectively. Specific absorption coefficient spectra, $a^*(\lambda)$ (m^2 mg^{-1} chl *a*), were calculated by dividing $a_{phy}(\lambda)$ by chl *a* concentration.

Inorganic carbon and nitrogen uptake

Experiments of inorganic carbon, nitrate and ammonium uptake were performed with samples collected at Stns A1, A5, B1 and B5. Samples obtained at the surface and SFM depth were incubated for 4 to 5 h in 1 l polycarbonate transparent bottles, in light-attenuated deck boxes, cooled by flowing surface seawater. Before the incubations the samples were prescreened through a 200 µm mesh and sodium bicarbonate-^{13}C (99 atomic % ^{13}C; 150 µM final concentration), potassium nitrate-N^{15} (99 at.% ^{15}N; 0.05 µM final concentration) or ammonium-N^{15} sulphate (98 at.% ^{15}N; 0.05 µM final concentration) was added. The final enrichment of dissolved inorganic carbon was 7%. The nitrate final enrichment calculated for the samples with nitrate concentrations above the detection limit varied from 1 to 55%. The final ammonium enrichment was 40% on average. Controls (i.e. samples without addition of ^{13}C or ^{15}N) were also incubated. The isotope enrichment and the concentration of particulate organic carbon (POC) and nitrogen (PON) was estimated at the beginning of the experiments by filtering 1 l of initial non-incubated seawater (i.e. without ^{13}C or ^{15}N added) through precombusted (450°C for 2 h) Whatman GF/F filters. After incubation, the samples were filtered through precombusted Whatman GF/F filters. The filters were frozen and stored until they were exposed to HCl fumes overnight and then dried and pelletized for isotopic analysis. Carbon and nitrogen stable isotope natural abundance measurements were made by continuous flow isotope-ratio mass spectrometry with a DELTA PLUS Finnigan MAT mass spectrometer. This technique also provided the POC and PON data.

The calculations of inorganic carbon uptake rates (µg m^{-3} h^{-1}) were performed following the method of Dugdale & Wilkerson (1986):

$$\text{C uptake} = [{}^{13}C_{s(t)} - {}^{13}C_{s(0)}] \times \text{POC} / ({}^{13}C_{enr} - {}^{13}C_{nat}) \times t^{-1} \quad (2)$$

where $^{13}C_{s(0)}$ and $^{13}C_{s(t)}$ are the atomic % ^{13}C excess at the beginning of (0) and after (t) the incubation period, $^{13}C_{enr}$ is the initially labelled fraction (7%), $^{13}C_{nat}$ is the percentage of dissolved ^{13}C occurring naturally and t is the incubation time in hours.

The calculations of nitrogen uptake were performed following the method of Knap et al. (1996). The initial PON concentration was used for the calculations, as it varied on average <10% after incubation. The main problem in calculating *in situ* uptake rates in our experiments was that the addition of ^{15}N increased the nitrogen concentration >10% in some samples. This could lead to an overestimation of the nitrogen uptake rates (Dugdale & Goering 1967). For these samples, the uptake rates were corrected following the procedure proposed by MacIsaac & Dugdale (1972). Another problem inherent to the ^{15}N uptake experiments is the possible change of the isotope enrichment of ammonium during incubation due to N regeneration (dilution effect). The potential underestimation of the NH_4^+ uptake rates was evaluated following the numerical procedure proposed by Kanda et al. (1987). It was assumed that uptake and regeneration rates were tightly coupled (i.e. a value of 1 for parameter *a* in Eq. [8] of Kanda et al. 1987 was assumed). According to the results of these calculations, the underestimation of the uptake rates was <5%. The relative nitrate uptake was estimated as the ratio between NO_3^- uptake and (NO_3^- + NH_4^+) uptake.

Statistical analysis

A principal component analysis (PCA) was performed in order to identify the main variation patterns among the physical and chemical variables (Savenkoff et al. 1995). The variables included in the analysis were temperature, salinity, nutrient concentrations (nitrate, ammonium, silicate and phosphate), nutrient molar ratios (nitrate:phosphate, N:P; nitrate:silicate, N:Si; silicate:phosphate, Si:P) and chl *a* concentration. Each variable was normalized to 0 mean by first subtracting the mean value for the whole data

set and then dividing it by the standard deviation. PCA was performed with the data obtained at the 10 stations at each sampling depth (excluding the data obtained below the ML). The scores of the 2 first components (PC1 and PC2) extracted from the PCA for each sample were used to research the relationships among the main hydrological patterns and the changes in composition and cell size of the phytoplankton communities. For this objective, the correlations among the biological variables (biomass of picoplankton, diatoms, dinoflagellates and flagellates, ESD of microplankton and diatoms) and the scores for PC1 and PC2 were analysed. The correlations were studied by Pearson's correlation analysis: p-values of the coefficient correlations were calculated in order to determine their statistical significance.

One-way ANOVA was performed in order to determine the statistical significance of the differences in diatom cell size, ratio of chl *a* to POC, light specific absorption coefficient and uptake rates of inorganic carbon, nitrate and ammonium between the coastal stations (A1 and B1) and offshore stations (B5 and B5). Additionally, Pearson's correlation analyses among the metabolic variables, biomass and ESD were performed in order to research the possible relationships among the composition, size and metabolism of the communities.

Prior to performing the statistical tests, normality and homogeneity of variances of the biological variables were assessed. Normality was evaluated from the normal probability plot of the residuals of each variable. Homogeneity of variances was tested with a Levene's test. The assumptions of the parametric correlations and ANOVA were satisfied by all the variables. The software package Statistica 7.1 (Statsoft, 1984–2005) was used for the statistical analysis.

RESULTS

Surface temperature increased sharply from the coastal stations to the centre of the basin (Fig. 2a). In contrast, the highest surface salinity (>37.5) was registered in the coastal stations while salinity was <36.5 at the offshore stations (Fig. 2b). Furthermore, the vertical profiles of salinity at the coastal stations (A1,

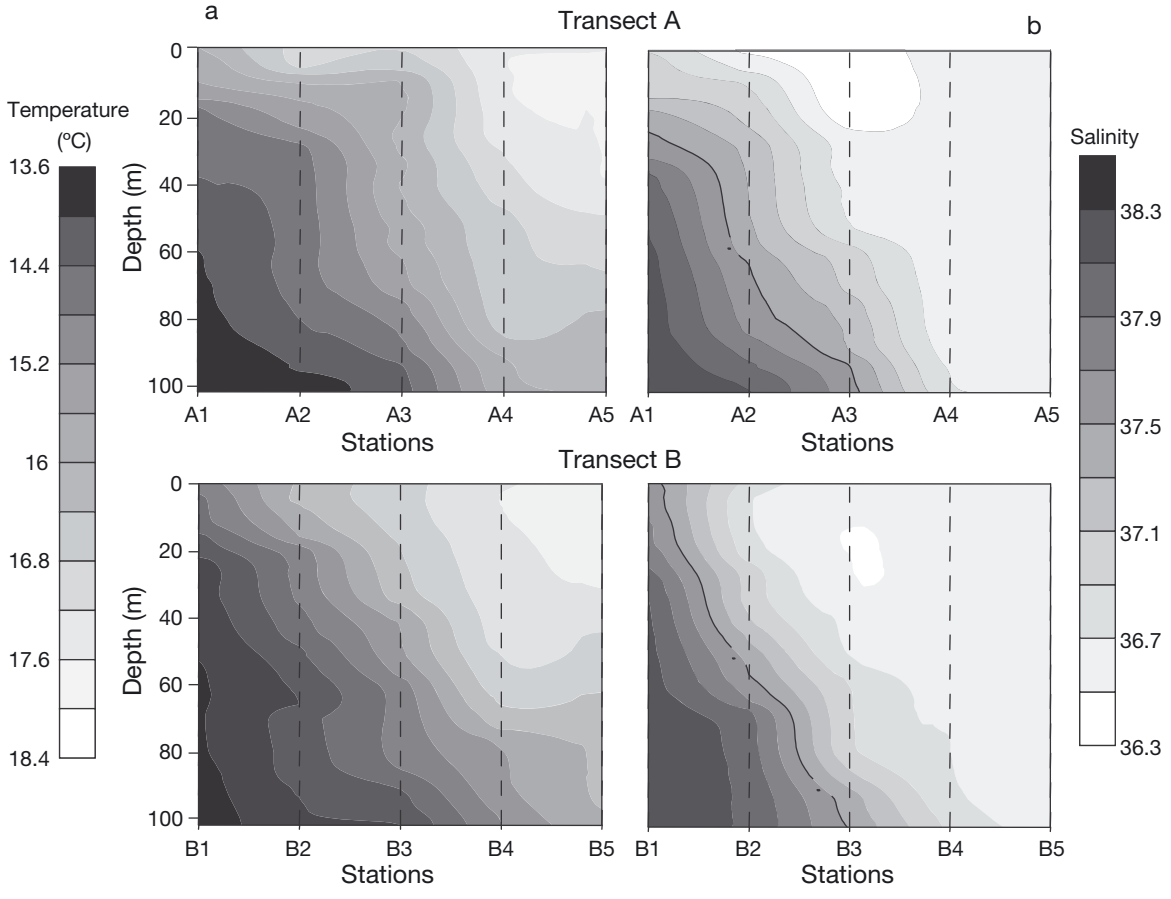

Fig. 2. Spatial variability in (a) temperature and (b) salinity along the 2 transects. Black isobar in (b) indicates salinity 37.5

A2, B1 and B2) indicated the presence of a strong vertical gradient of salinity located at depth 30–40 m. The gradient was deeper at the offshore stations (80–100 m; Stns A4, A5, B4, B5). Consequently, the vertical maximum of the Brunt Väisälä frequency (which indicates the pycnocline position) in the offshore stations was located at a higher depth in comparison with the coastal stations (Fig. 3). Concordantly, the thickness of the upper ML, estimated as the depth at which the potential density changed by 0.5 from that at the surface, was shallower in the coastal stations (Fig. 3). These differences in the hydrological features suggest that Stns A1, A2, B1 and B2 were affected by upwelling of deep water during the survey, whereas Stns A4, B4, A5 and B5 were located within the core of the western Alboran anticyclonic gyre. Coincidently, wind records at the study area indicate that westerly winds (that favour the coastal upwelling) started to blow 2 d prior to the samplings and were predominant during the survey (data not shown).

Surface concentrations of nitrate and phosphate decreased from the coast to offshore (Fig. 4). The highest concentrations of both nutrients were obtained at the stations where upwelling was more intense (i.e. Stns A1, A2, B1 and B2). In contrast, the surface concentrations were lower than the detection limit in the offshore stations (A4, B4, A5 and B5).

Chl *a* concentration in the surface layer decreased from the coast to offshore in the 2 transects (Fig. 5). A subsurface maximum of chl *a* fluorescence was detected at all stations although it became progressively deeper and less intense as the distance from the coast increased. Chl *a* concentration at the SFM depth varied from 2.6 µg l^{-1} at the coastal stations to 0.3 µg l^{-1} at the offshore stations. The SFM was located within the ML at the 10 sampling stations. However, the irradiance at SFM decreased from the coast to offshore. Thus, the SFM was located at 10%-I_0 depth at Stns A1, A2, A3, B1 and B2 and close to the euphotic layer lower limit (i.e. 1%-I_0 depth) at Stns A4, A5, B4 and B5 (Fig. 3).

The results of the PCA performed with the hydrological and chemical variables are shown in Fig. 6. The 2 first principal components (PC1 and PC2) explained 67% of the variability. Temperature and salinity were correlated with PC1 although with opposite signs (Fig. 6a). Consequently, PC1 represented the horizontal hydrological gradient from coastal to offshore stations. As expected, the nutrient concentrations and their molar ratios (except the Si:P molar ratio) were negatively correlated with PC1, corroborating that the upwelling of subsurface Mediterranean water produced enrichment of the ML at the coastal stations. Concordantly, Stns A1 and B1 had the most negative scores for PC1 (Fig. 6b). Stns A5 and B5 had positive (or slightly negative) scores for this variance component (with the exception of B5 at 100 m depth). The variability explained by PC2 was 12.5%. Ammonium and chl *a* concentrations were negatively correlated with PC2 (note that

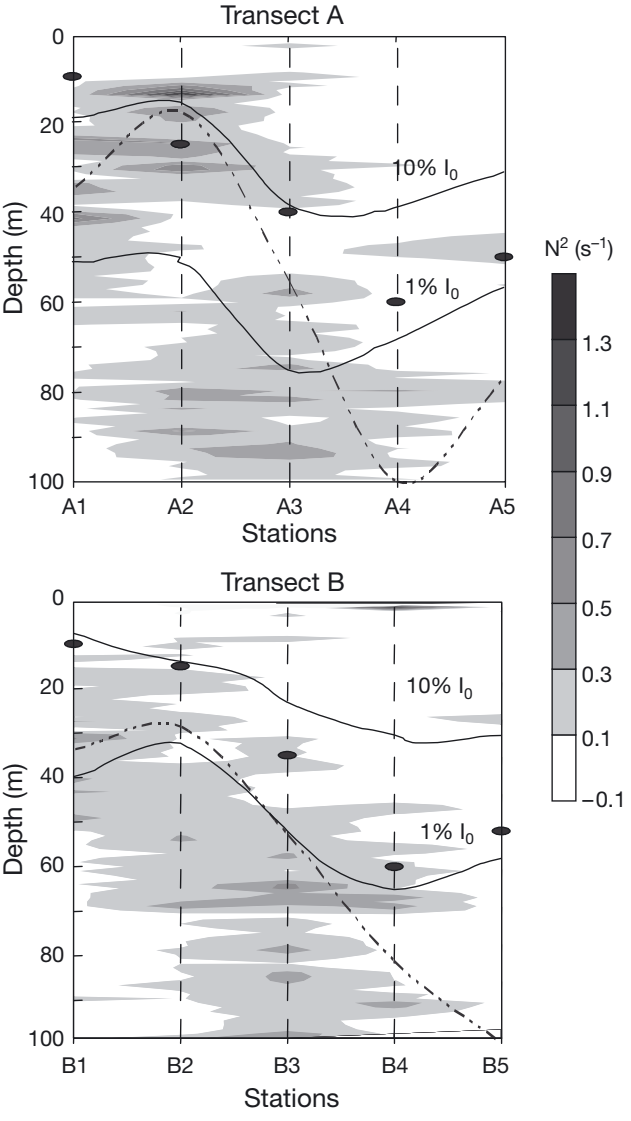

Fig. 3. Spatial variability in Brunt-Väisälä frequency (N^2) estimated from the potential density profiles for the 2 transects. Dash-dotted line shows the position of the lower limit of the mixed layer calculated as the depth at which the density difference from the surface was 0.5. Continuous black line shows the depths at which 10 and 1% of surface incident light (I_0) was reached. Black points show the position of the subsurface chl *a* fluorescence maximum (SFM) where samples for analysis of taxonomic and physiological features of the phytoplankton were collected

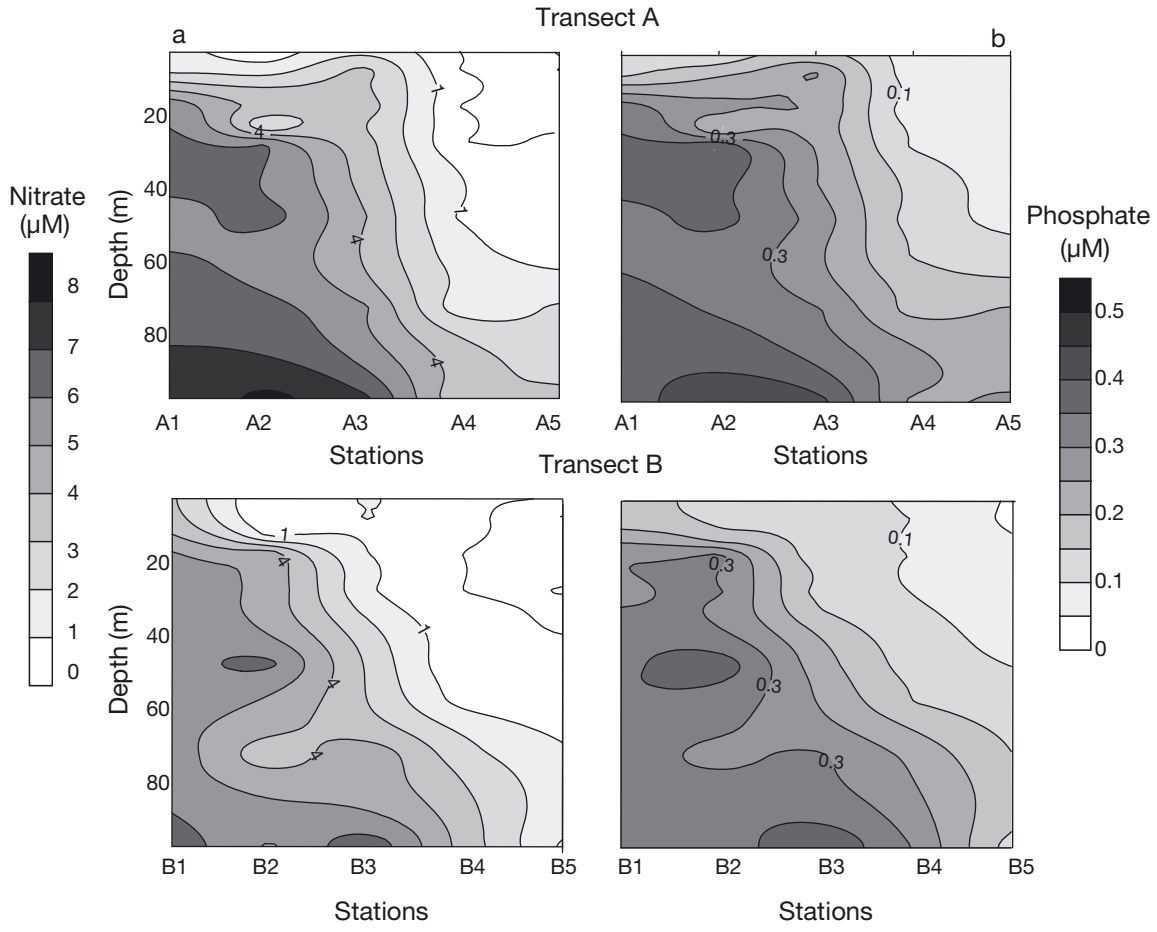

Fig. 4. Spatial variability in (a) nitrate and (b) phosphate along the 2 transects

chl *a* concentration was weakly correlated with PC1), however, optical depth was positively correlated with PC2. Surface samples collected at Stns A1, A2, B1 and B2 had the most negative scores for PC2, while the samples collected below 20 m depth had positive scores. Furthermore, most of the samples collected at Stns A3, A4, A5, B3, B4 and B5 had positive scores for PC2 (with the exception of deeper samples collected at Stn B5). Based on these results, it can be assumed that PC1 and PC2 gathered most of the surface samples of the stations affected by upwelling.

Distribution of the phytoplankton abundance

The 3 groups of picoplankton presented distinguishing horizontal and vertical distribution patterns (Fig. 7). The maximal abundances of *Prochlorococcus* were obtained at the central stations of the 2 transects, although the vertical distribution range was wider at Stns A3 and A4 (between 20 and 80 m depth) than at Stn B3 (where its abundance decreased sharply below 40 m depth; Fig. 7a). The highest abundances of *Synechococcus* were found between 20 and 30 m depth at the offshore stations (A4, A5, B4 and B5; Fig. 7b). The abundance of picoeukaryotes (and nanoeukaryotes) followed horizontal and vertical distribution patterns similar to those described for chl *a* (Fig. 7c,d), as the highest abundances of both groups were obtained in the surface layer of the coastal stations (A1, A2, B1 and B2).

The highest abundances of microplankton and diatoms were obtained at Stn B2, although abundances of both cell groups decreased from the coast to offshore in the 2 transects (Fig. 8). Flagellates abundances tended to also be higher at the coastal stations in comparison with the offshore stations, especially in transect B. The highest abundance of dinoflagellates was obtained at the SFM depth at Stn B2, though a clear horizontal variability pattern from the coast to offshore was not obtained for this group. Diatom cells were the most abundant in all the samples analysed, with the exception of the surface samples of Stns A4, B4 and B5 and the SFM samples of

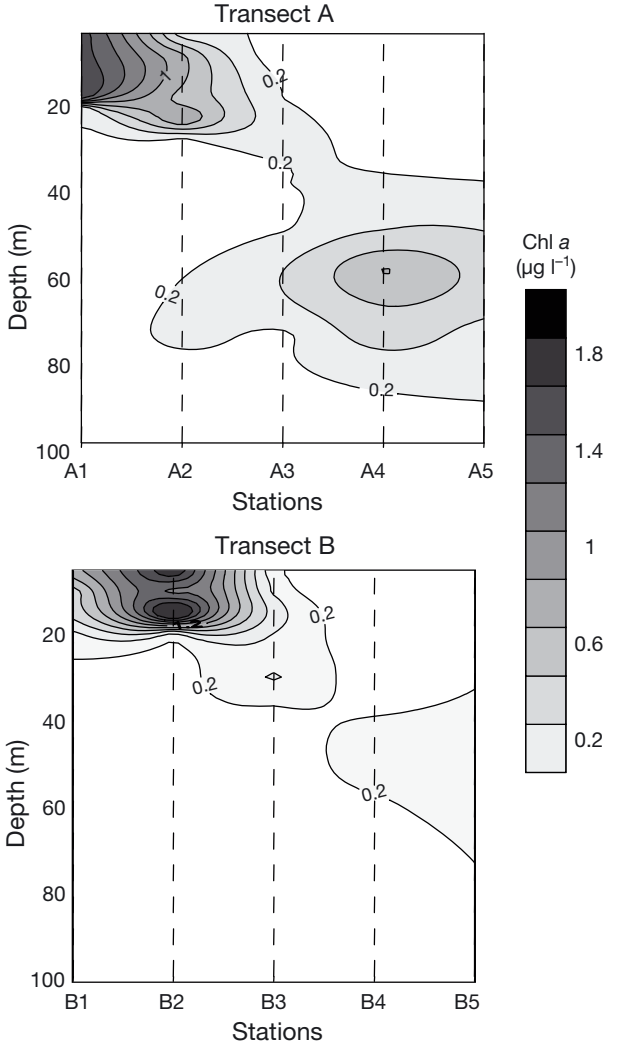

Fig. 5. Spatial variability of chl *a* concentration along the 2 transects

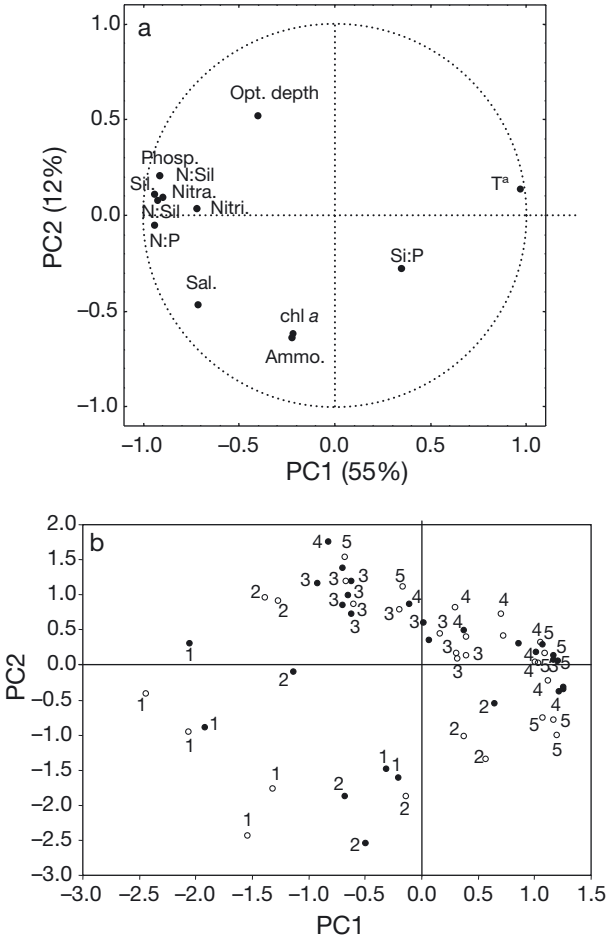

Fig. 6. (a) Structure of the 2 first principal components extracted from the PCA performed with temperature (T^a), salinity (Sal.), nitrate (Nitra.), nitrite (Nitri.), ammonium (Ammo.), silicate (Sil.), phosphate (Phosp.), nitrate to phosphate molar ratio (N:P), nitrate to silicate molar ratio (N:Si), silicate to phosphate molar ratio (Si:P), chlorophyll *a* (chl a) and optical depth (Opt. depth). (b) Scores for PC1 and PC2 of each sample that was included in the analysis. The numbers indicate the station (black points, transect A; white points, transect B)

Stns A5 and B3 which were dominated by flagellates. There were no samples dominated (in terms of abundance) by dinoflagellates.

The results of the correlation analyses among abundances of the phytoplankton groups and scores for PC1 and PC2 support the differences among the horizontal and vertical distribution patterns described above. Abundance of *Synechococcus* was positively correlated with the scores for PC1 (Table 1). This result corroborates that *Synechococcus* was more abundant in the warmer and less salty waters of the offshore stations. The correlations between scores for PC2 and abundances of pico- and nanoeukaryotes, diatoms and flagellates were statistically significant, probably because higher abundances of these 4 groups co-occurred in the surface layer of the coastal stations. Furthermore, abundance of <50 µm diatoms and ratio of diatoms to dinoflagellates was negatively correlated with both scores for PC1 and PC2. In contrast, abundances of *Prochlorococcus* and dinoflagellates were not significantly correlated with the scores for PC1 or PC2 indicating that their distribution patterns were not clearly related to the hydrological patterns identified by the PCA.

Size structure of the phytoplankton communities

In most of the samples analysed, the diatoms covered a wide range of cell length, from 14 to 140 µm ESD. However, the mean length of the dominant spe-

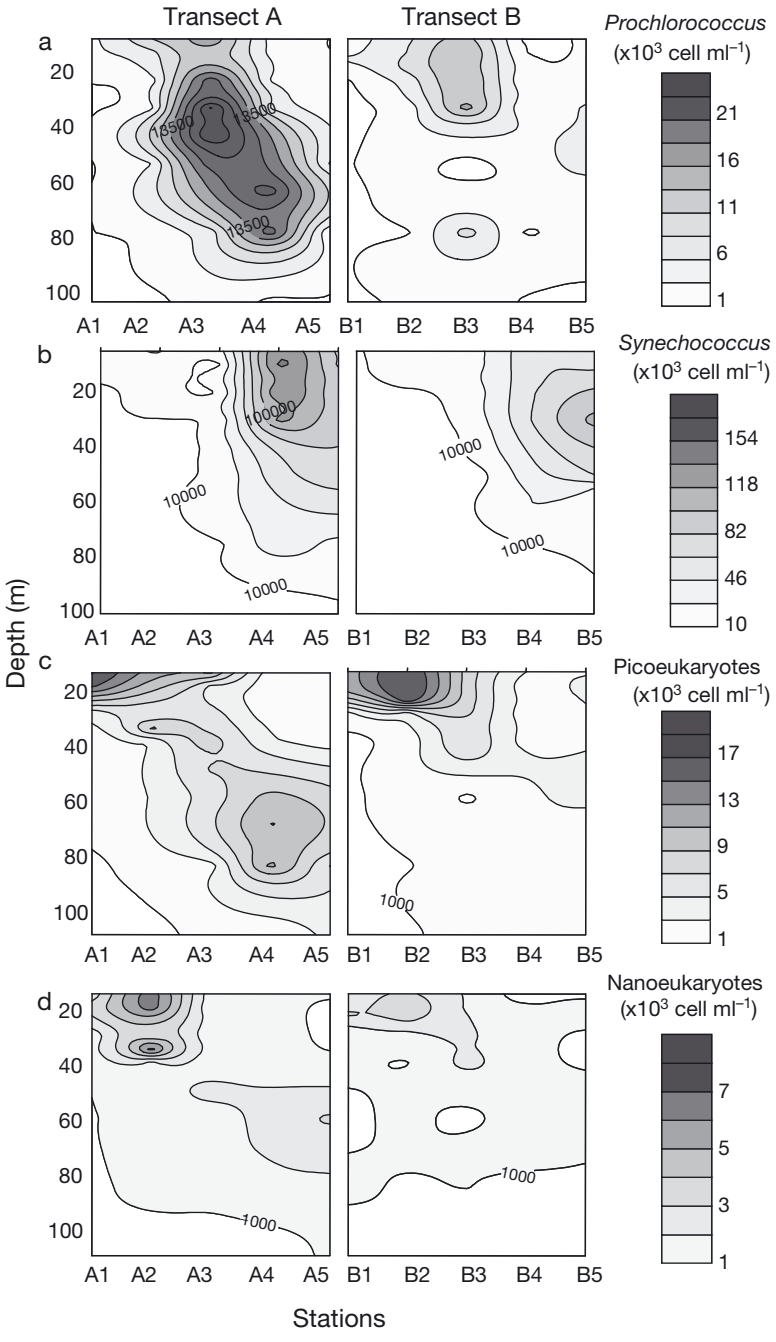

Fig. 7. Spatial variability in the abundance of (a) *Prochloroccocus*, (b) *Synechococcus*, (c) picoeukaryotes and (d) nanoeukaryotes quantified by means of flow cytometry along the 2 transects

cies differed between the coastal and offshore stations. The diatom community in the coastal stations was dominated by *Chaetoceros*, *Asterionellopsis* and *Leptocylindrus minimum* with ESD lower than 50 µm. At the offshore stations, the diatom community was dominated by large diatoms (>50 µm ESD) of the genus *Leptocylindrus* and other species of the genera *Nitzschia* and *Pseudonitzschia*. Consequently, the mean ESD for the diatom community was about 40% lower at Stns A1, A2, B1 and B2 than at Stns A4, A5, B4 and B5 (Fig. 9, Table 2). In contrast, ESD averaged for flagellates and dinoflagellates did not change significantly from the coast to offshore (data not shown). ESD averaged for the whole microplankton community (i.e. including diatoms, flagellates and dinoflagellates) followed the same variability pattern as the one obtained for diatoms, although the differences between the coastal and offshore stations were not statistically significant (Table 2). ESD averaged for both microplankton and diatoms were positively correlated with the scores for PC1 (Table 1). Therefore, the changes in cell length of the microplankton communities were mainly related to changes in size structure of the diatom community along the coast– offshore hydrological gradient.

In order to estimate the contribution of each phytoplankton group to the whole community, cell abundances were transformed into equivalent biomass and afterwards the biomass percentage in relation to phytoplankton total biomass was quantified (Fig. 10). *Prochlorococcus* counted for less than 1% of the phytoplankton biomass (note that the *x*-axis scale in Fig. 10 hampers the visualization of the *Prochlorococcus* biomass percentage). *Synechococcus* biomass percentage was maximal in the surface sample of Stn A4 and minimal in the surface sample of Stn B1. Concordantly, *Synechococcus* biomass percentage and scores for PC1 were positively correlated (Table 1). Picoeukaryote biomass percentage was comparatively lower in transect B, although it tended to decrease at the offshore stations of the 2 transects. As described for cell abundance, the diatoms were the dominant group in terms of biomass at the coastal stations (A1, A2, B1 and B2; Fig. 10). In contrast, the community was dominated by dinoflagellates at the offshore stations. Consequently, diatom biomass percentage was negatively correlated with the scores for PC1 while dinoflagellate biomass percentage was positively correlated (Table 1). Interestingly, small diatom biomass percentage (ESD <50 µm) was sig-

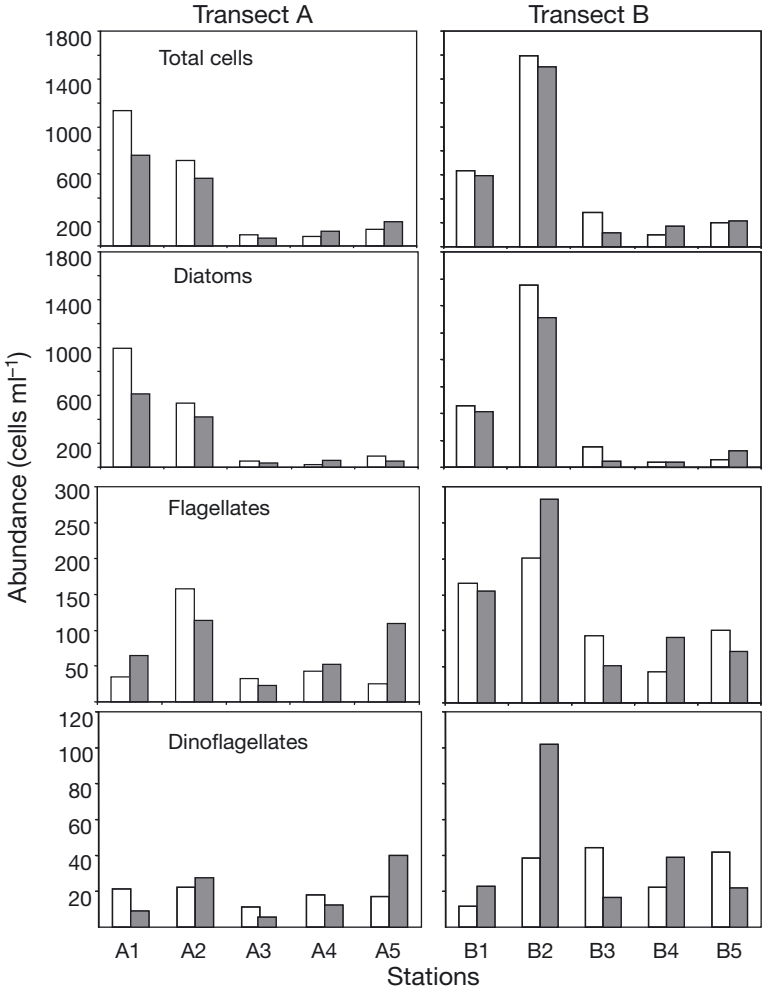

Fig. 8. Abundance of microplankton cells (total cells estimated as the sum of diatoms, flagellates and dinoflagellates), diatoms, flagellates and dinoflagellates in the samples collected at the surface (white columns) and at the subsurface chl *a* fluorescence maximum depth (SFM; grey columns) of the 10 sampling stations

nificantly correlated with the scores for PC1, but the correlation between large diatom biomass percentage and scores for PC1 was not statistically significant. Therefore, the differences in diatom biomass along the coast–offshore gradient were mainly due to changes in the abundance of the smaller diatoms. Biomass percentages of *Prochlorococcus*, nanoplankton and dinoflagellates were positively correlated with the scores for PC2, whereas the correlation between the scores for PC2 and diatom biomass was negative.

In order to visualize how the changes in the community composition affected the size structure, the biomass percentages by different cell size classes were calculated (Fig. 11, only data of Stns A1, A5, B1 and B5 are shown). For these comparisons, size classes relative to cell biovolume were used instead of ESD. The main difference in the distribution of biomass percentages by size classes between coastal and offshore stations was a drastic reduction in the biomass of the 100 to 1000 µm^3 size class, mostly in <50 µm diatoms. Furthermore, in the samples collected at offshore stations, the 10^3– 10^4 µm^3 size class counted for >70% of the phytoplankton biomass.

Physiological features of the phytoplankton communities

In our study, cell content of chl *a* was indirectly estimated from the ratio of chl *a* to POC. Chl *a*: POC (Fig. 11a) ranged from 5 to 41 µg chl *a* mg^{-1} POC obtained in the surface samples of Stns B5 and B1, respectively. Furthermore, chl *a*:POC was significantly higher at the coastal stations in comparison with the offshore stations (Table 2). The highest $a^*(440)$ value (0.08 m^2 mg^{-1} chl *a*) was also obtained in the surface sample of Stn B5, although the differences between coastal and offshore stations were not statistically significant (Fig. 12b). In order to research which phytoplankton group contributed to these differences in chl *a*:POC and $a^*(440)$, correlation analyses among these 2 variables and biomass percentages for each group were performed (Table 3). Chl *a*:POC was negatively correlated with *Synechococcus* biomass percentage and positively with <50 µm diatom biomass percentage. The correlation between <50 µm diatom biomass percentage and $a^*(440)$ was also significant although negative. In contrast, $a^*(440)$ was positively correlated with the biomass percentages of *Synechococcus*, nanoplankton and dinoflagellates.

The biomass-specific rates of carbon uptake (*V*DIC) were about 4-fold higher in the coastal samples in comparison with the offshore samples (Fig. 12c, Table 2). The variability in the biomass-specific nitrate uptake rates (VNO_3^-) was substantial among the 8 samples analysed, although on average VNO_3^- was also significantly higher at the coastal stations (Fig. 12d, Table 2). In contrast, the biomass-specific ammonium uptake rates (VNH_4^+; Fig. 12e) were higher in the offshore samples even though the differences between the coast and offshore were not statistically significant (Table 2). VNH_4^+ at the coastal

Table 1. Pearson's correlation coefficients of the correlations among the scores for the 2 first principal components extracted from the PCA (PC1 and PC2) and the cell abundances of each group (microplankton is the sum of diatoms, dinoflagellates and flagellates; Diat/Dino is the ratio of diatom to dinoflagellate), their biomass percentages (i.e. the biomass of each group normalized by the total phytoplankton biomass), and the equivalent spherical diameter (ESD) averaged for the microplankton and diatoms. Coefficients statistically significant are in **bold** (*p < 0.05; **p < 0.01). N indicates the number of samples used in each comparison

	PC1	PC2	N
Cell abundances			
Prochlorococcus	−0.08	0.23	57
Synechococcus	**0.79****	−0.08	57
Picoeukaryotes	−0.08	**−0.52****	57
Nanoeukaryotes	−0.06	**−0.57****	57
Microplankton	0.01	**−0.72****	20
Diatoms	−0.24	**−0.71****	20
<50 µm diatoms	**−0.57****	**−0.73****	
>50 µm diatoms	0.02	**−0.46***	
Flagellates	0.29	**−0.74****	20
Dinoflagellates	0.16	−0.28	20
Diat/Dino	**−0.40***	**−0.63****	20
Biomass percentage			
Prochlorococcus	−0.23	**0.48***	20
Synechococcus	**0.56****	0.33	20
Picoeukaryotes	0.28	0.41	20
Nanoplankton	−0.23	**0.50***	20
Microplankton	0.11	**−0.58****	20
Total diatoms	**−0.48***	**−0.75****	20
<50 µm diatoms	**−0.57****	**−0.73****	20
>50 µm diatoms	0.02	**−0.47***	20
Flagellates	−0.25	0.28	20
Dinoflagellates	**0.53****	**0.72****	20
Cell size (ESD)			
Microplankton	**0.45***	0.07	20
Diatoms	**0.66****	−0.11	20

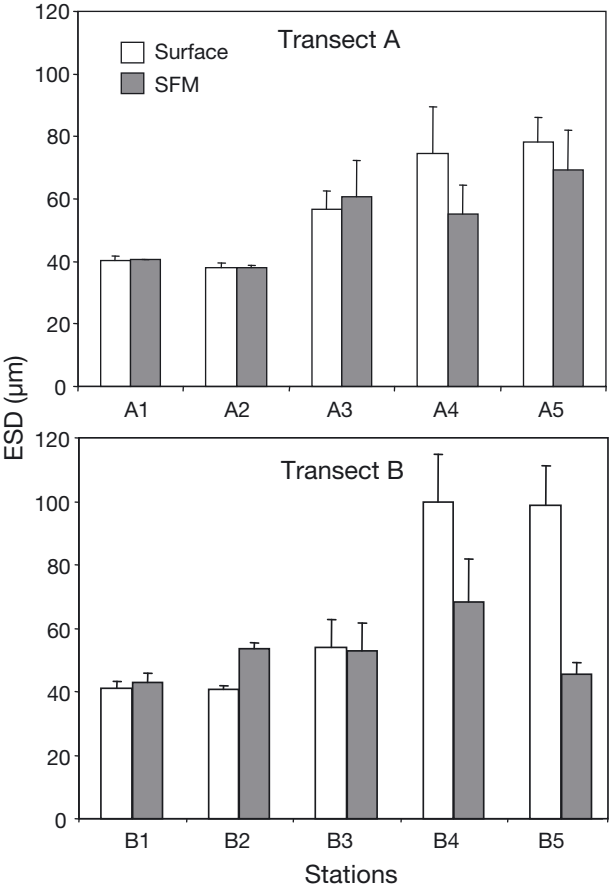

Fig. 9. Average values of the equivalent spherical diameter (ESD) of the diatom community in the samples collected at the surface (white columns) and at the subsurface chl *a* fluorescence maximum depth (SFM; grey columns) of the 10 sampling stations. Error bars indicate +1 SE

stations was 5 to 20-fold lower than $V\mathrm{NO_3^-}$. On the contrary, $V\mathrm{NH_4^+}$ was higher than $V\mathrm{NO_3^-}$ at the offshore stations. The coefficients for the correlations among uptake rates and biomass percentages of the phytoplankton groups are showed in Table 3. Biomass percentage of <50 µm diatoms was positively correlated with *V*DIC and $V\mathrm{NO_3^-}$ and negatively with $V\mathrm{NH_4^+}$. Furthermore, picoeukaryote biomass percentage was correlated with *V*DIC and $V\mathrm{NH_4^+}$ and biomass percentages of *Synechococcus* and dinoflagellates were negatively correlated with *V*DIC.

DISCUSSION

Hydrological variability, nutrients and chl *a*

The surface layer at the western sector of the Alboran Sea is usually occupied by Modified Atlantic Water (MAW) with 36.5 salinity and low nutrient con-

Table 2. One-way ANOVA performed to determine the statistical significance of the differences in cell length and physiological features between the coastal communities (data obtained at the surface and sub-surface chl *a* fluorescence maximum (SFM) depth of Stns A1 and B1) and the offshore communities (surface and SFM samples of Stns A5 and B5). ESD, equivalent spherical diameter; $a^*(440)$, chl *a* specific absorption coefficient at 440 nm; *V*DIC, $V\mathrm{NO_3^-}$ and $V\mathrm{NH_4^+}$, biomass-specific uptake rates of dissolved inorganic carbon, nitrate and ammonium, respectively. **Bold** indicates significant differences at p < 0.05

	F	p
Microplankton ESD	2.4	0.14
Diatom ESD	**21.1**	<0.001
$a^*(440)$	7.6	0.05
chl *a*/POC	**12.2**	0.01
*V*DIC	**144.9**	<0.001
$V\mathrm{NO_3^-}$	**7.2**	0.004
$V\mathrm{NH_4^+}$	5.4	0.06

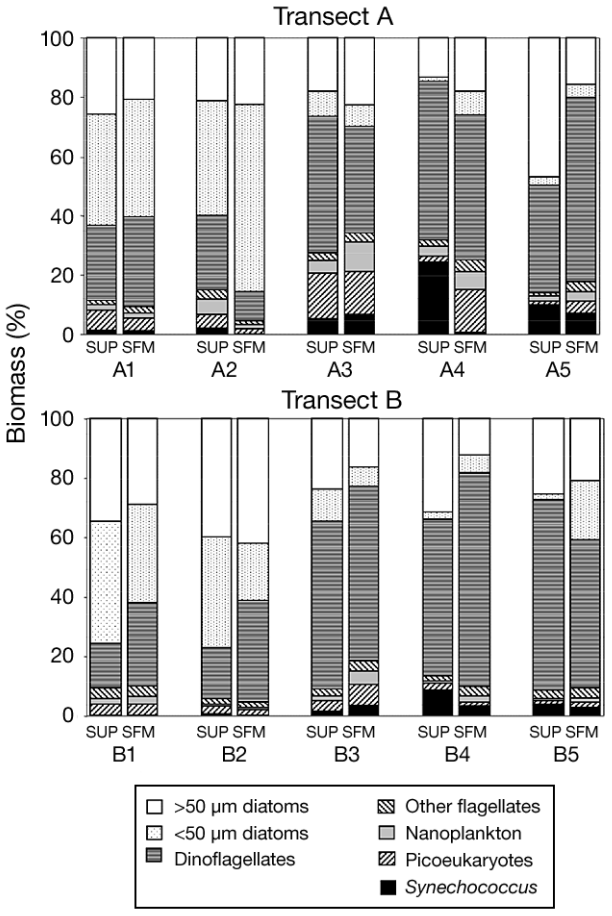

Fig. 10. Biomass percentages of the main groups of phytoplankton in the samples collected at the surface (SUP) and at the subsurface chl *a* fluorescence maximum depth (SFM) of the 10 sampling stations

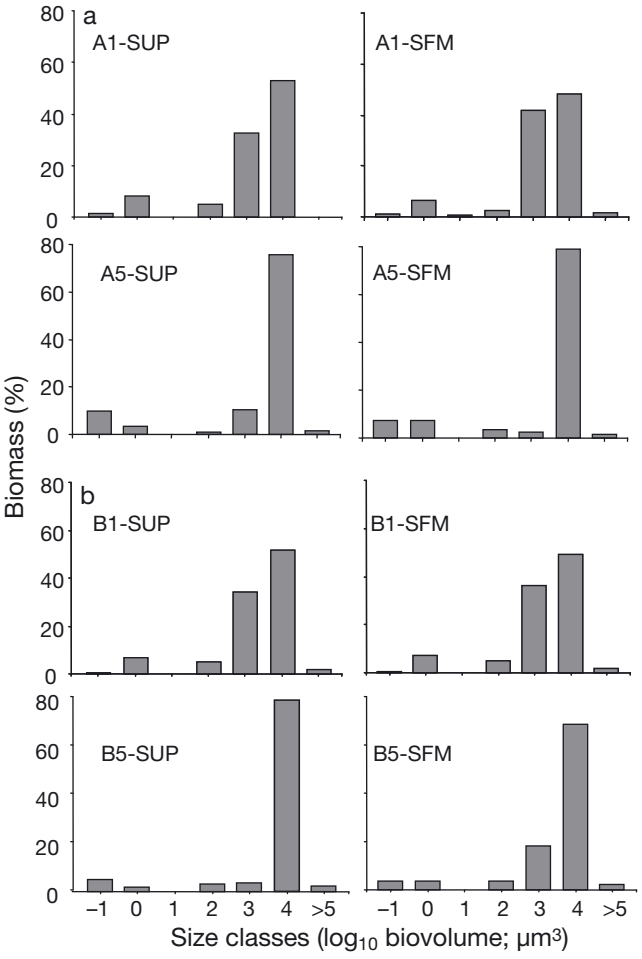

Fig. 11. Biomass percentages of the different size classes of phytoplankton in the samples collected at the surface (SUP) and the subsurface chl *a* fluorescence maximum depth (SFM) of the coastal (A1 and B1) and offshore (A5 and B5) stations. The *x*-axis labels indicate the higher limits of each biovolume size class

centration (Minas et al. 1991, Rodríguez et al. 1997). However, saltier and colder waters are frequently detected along the northern coast of the Alboran Sea due to subsurface Mediterranean water upwelling driven by westerlies (Minas et al. 1991, Lafuente et al. 1998, Rodríguez et al. 1998, Sarhan et al. 2000, Ramírez et al. 2005, Mercado et al. 2007). Westerly winds started to blow 2 d prior the samplings presented in this report. Therefore, it is probable that the nutrient enrichment and the decrease in the upper mixed layer thickness measured at the coastal stations were due to upwelling of Mediterranean water. In contrast, salinity values in the surface layer of the offshore stations were similar to those described in the literature for the MAW. The thickness of the MAW layer was almost 100 m at Stns A4, A5, B4 and B5, indicating that these stations were located within the western Alboran anticyclonic gyre core (Parrilla & Kinder 1987).

Our data show that the upwelling modified the availability of resources for phytoplankton growth (nutrients and irradiance) at the coastal stations in comparison with the offshore stations. On average, nitrate concentration in the ML of the coastal stations was 6-fold higher than at the offshore stations, while silicate and phosphate concentrations were 2.5-fold higher. Consequently, the upwelling produced an increase in nitrate relative to silicate and phosphate concentration that is attributable to the different nutrient composition of the upwelled Mediterranean water (Dafner et al. 2003, Ramírez et al. 2005, Reul et al. 2005). In addition, the light conditions in the water column were modified by the upwelling because the phytoplankton cell displacement underneath the first optical depth layer (20–30 m) must have been ham-

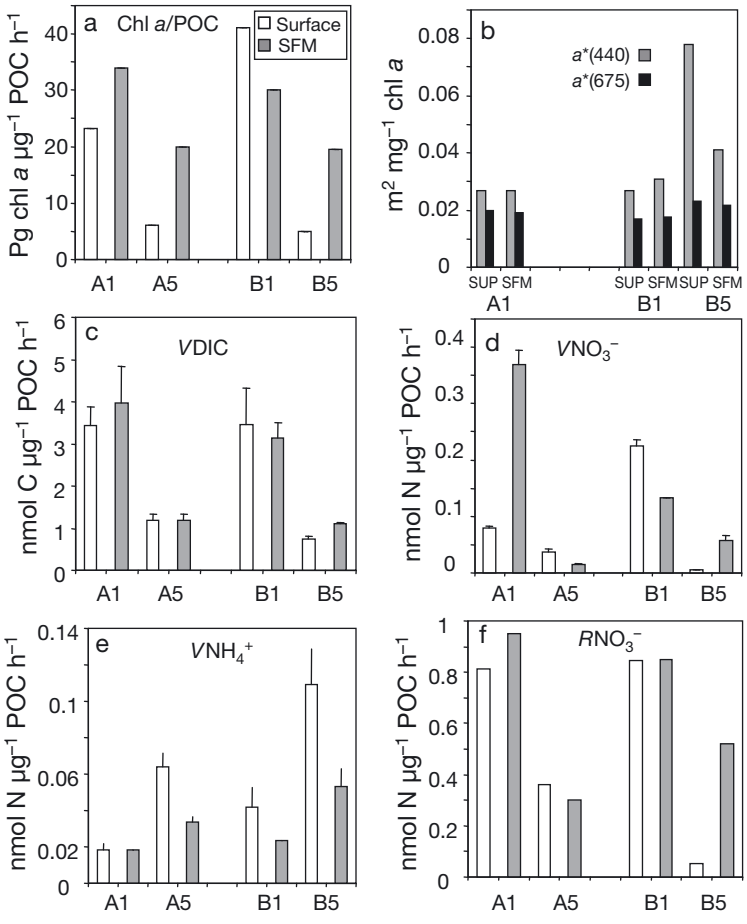

Fig. 12. Physiological performances of the phytoplankton communities measured at the coastal (A1 and B1) and offshore (A5 and B5) stations. Except in panel b, white and grey columns indicate the results for samples collected at the surface (SUP) and subsurface chl *a* fluorescence maximum depth (SFM), respectively. (a) Chl *a*/POC, ratio of chl *a* to particulate organic carbon concentration; (b) $a^*(440)$ and $a^*(675)$, chl *a* specific absorption coefficient at 440 and 675 nm, respectively; (c) *V*DIC, biomass-specific dissolved inorganic carbon uptake rate; (d) $V\mathrm{NO_3^-}$, biomass-specific nitrate uptake rate; (e) $V\mathrm{NH_4^+}$, biomass-specific ammonium uptake rate; (f) $R\mathrm{NO_3^-}$, nitrate relative to (nitrate + ammonium) uptake rate. Error bars indicate +1 SD. Note that there are no available data for $a^*(440)$ or $a^*(675)$ at Stn A5

pered by the reduction of the ML thickness. In contrast, the ML thickness (70–80 m) at the offshore stations in combination with the vertical surface water downwelling caused by the circulation pattern in the anticyclonic gyre core would permit phytoplankton cell displacement below the first optical depth layer.

As expected, the highest chl *a* concentrations of the ML were obtained at the coastal stations where the nutrient availability was also relatively high. However, the correlation between chl *a* and salinity, temperature and nutrient concentration was weak as revealed by the structure of the first principal component extracted from the PCA (Fig. 6). The lack of correlation between chl *a* and nutrients could be partially due to consumption by phytoplankton. This was particularly noticeable in Stn B2 where the highest concentration of chl *a* was obtained although the nitrate concentration was relatively low. However, the chl *a* concentration was low in the surface layer of Stn B3 despite high nutrient concentrations. These findings suggest that nutrient availability was not the only prerequisite for stimulating phytoplankton growth. In fact, the results of the PCA hint that the phytoplankton bloom was jointly triggered by the nutrient enrichment and ML thickness decrease. This conclusion is in agreement with previous observations performed at the Alboran Sea (Claustre et al. 1994, Morán & Estrada 2001, Ramírez et al. 2005) and broadly supports the hypothesis of Sverdrup (1953) that bloom initiation is produced when the surface mixed layer becomes shallower.

Effects of hydrological variability on abundance and composition of the phytoplankton communities

The 3 groups of picoplankton analysed presented different horizontal distribution patterns. Higher abundances of *Synechococcus* were obtained at the stations occupied by MAW, whereas *Prochlorococcus* was more abundant at intermediate depths at the stations with surface salinity values and nutrient concentrations midway between those featuring the MAW and the upwelled Mediterranean water. Picoeukaryotes were more abundant in the recently upwelled surface waters of the coastal stations, indicating that they responded more rapidly than *Prochlorococcus* and *Synechococcus* to the changes induced by upwelling. These distribution patterns fit only partially to the ones described by Reul et al. (2005) for the same study area, as these authors determined that both *Prochlorococcus* and *Synechococcus* increased in the western Alboran oligotrophic gyre in comparison to the northern coastal area. In the eastern Alboran Sea, Jacquet et al. (2010) also found that the picoplankton community was dominated by *Synechococcus* in the anticyclonic gyre while *Prochlorococcus* dominated at intermedi-

Table 3. Pearson's correlation coefficients obtained from comparisons between physiological variables and biomass percentages of the different phytoplankton groups (chl *a*/POC, ratio of chl *a* to particulate organic carbon; $a^*(440)$, chl *a* specific absorption coefficient at 440 nm; *V*DIC, $V\mathrm{NO_3^-}$ and $V\mathrm{NH_4^+}$, biomass-specific uptake rates of dissolved inorganic carbon, nitrate and ammonium, respectively). The correlation coefficients between mean cell length of microplankton and diatoms and the physiological variables are also shown (ESD, equivalent spherical diameter). Coefficients statistically significant are in **bold** ($^*p < 0.05$; $^{**}p < 0.01$). N was 8 for all comparisons

	chl *a*/POC	$a^*(440)$	*V*DIC	$V\mathrm{NO_3^-}$	$V\mathrm{NH_4^+}$
Biomass					
Prochlorococcus	0.003	0.20	−0.28	−0.34	−0.30
Synechoccocus	**−0.75***	**0.87***	**−0.74***	−0.61	0.41
Picoeukaryotes	0.57	−0.72	**0.73***	0.36	**−0.81***
Nanoplankton	−0.34	**0.81***	0.10	0.04	−0.66
<50 µm diatoms	**0.88****	**−0.97****	**0.94****	**0.77***	**−0.71***
>50 µm diatoms	0.20	0.20	0.01	−0.06	0.22
Dinoflagellates	−0.70	**0.90***	**−0.84****	−0.63	0.59
Flagellates	0.50	0.09	0.06	0.1	0.11
Cell size (ESD)					
Microplankton	−0.54	0.12	−0.34	−0.29	0.14
Diatoms	**−0.85****	**0.98****	**−0.79***	−0.63	**0.85****

ate depths (ca. 30 to 100 m) in the edge of this gyre. Jacquet et al. (2010) attributed the distribution pattern of *Synechococcus* at the eastern Alboran Sea to the horizontal gradient of nutrients, which is in agreement with the widely accepted paradigm that *Synechococcus* grows optimally in nutrient enriched and mixed waters. However, Reul et al. (2005) demonstrated that *Synechococcus* abundance in the western sector of the Alboran Sea was negatively correlated with nutrient concentrations, which is corroborated by the results of the present study.

Contribution of picoplankton to phytoplankton biomass at the offshore stations varied from 11 to 26%. These figures are similar to those reported by Reul et al. (2005) for the western Alboran Sea in spring. Picoplankton biomass percentage was slightly lower at the coastal stations mainly due to lower abundance of *Synechoccocus*. These changes were reflected in a higher biomass percentage of cells smaller than 1 μm^3 in biovolume at offshore stations in comparison with coastal stations. However, the most conspicuous horizontal variability pattern in the size structure of the communities from the coast to offshore was obtained for the size classes higher than 10^3 μm^3 in biovolume (that roughly included cells greater than 10 µm in length). Particularly, the biomass percentage of 10^3–10^4 μm^3 biovolume cells drastically reduced along the coast–offshore gradient. These changes paralleled an increase in the ESD of the microplankton community. No differences in the ESD of flagellates or dinoflagellates were attributable to the hydrological gradient. However, ESD of diatoms was positively correlated with the first factor extracted from the PCA, which can be attributed to high abundance of <50 µm diatoms in comparison with >50 µm diatoms at the coastal stations. Consequently, our data demonstrate that changes in cell size along the coast–offshore gradient were due to changes in the abundance of diatoms relative to dinoflagellates.

Sampling started just 2 d after westerly winds began to blow and this wind regime predominated during the survey. Consequently, it can be hypothesized that the communities sampled at the coastal stations represented a relatively early phase of the phytoplankton bloom induced by upwelling. According to Mercado et al. (2005, 2011), diatom communities in the northwestern Alboran Sea during this bloom phase are dominated by *Chaetoceros*, which is consistent with the results of the present study. Moreover, our results support the paradigm that diatoms dominate the phytoplankton community in areas affected by upwelling, although the outcomes of this study indicate that <50 µm diatoms responded more rapidly than the other size classes to the upwelling-induced changes. In contrast, the diatom communities in the offshore stations were dominated by *Leptocylindrus*, *Asterionellopsis* and *Rhizosolenia* with relatively large ESD. Chl *a* satellite images for the sampling days indicate that the chlorophyll produced at the upwelling area was displaced towards the east by the current induced by the Atlantic jet, away from the offshore stations. Consequently, it is improbable that these large cells reached the offshore stations by advection from the coastal areas. This predominance (in terms of biomass) of large cells at the offshore stations apparently contradicts the widely accepted paradigm that small cells dominate the phytoplankton community in oligotrophic areas (Azam et al. 1983, Goldman 1993).

Relationship between phytoplankton composition and metabolic rates

In our study, the changes in community composition were correlated with variations in the efficiency of light absorption, which was higher in the offshore

communities (dominated by dinoflagellates) in comparison with the coastal communities (dominated by <50 µm diatoms). Differences in light absorption efficiency per chl *a* unit among marine phytoplankton assemblages have been attributed to the distinguishing pigment composition of the taxonomic groups that shape the community (Hoepffner & Sathyendranath 1991) and/or to changes in the effect of pigment packaging (that diminishes their light absorption efficiency). The pigment packaging effect is modulated by the cell size and shape traits and by the pigment intracellular content. In particular, the packaging effect increases with cell size (Ciotti et al. 2002, Ciotti & Bricaud 2006) and lessens with decreasing pigment internal content (Thompson et al. 1992, Reynolds et al. 1997, Stramski et al. 2002). In our study, changes in taxonomic composition, cell ESD (and biovolume) and chl *a* per biomass (that is a proxy for the average chl *a* cell content for the community) co-varied along the coast–offshore gradient; therefore, it is difficult to isolate the factor which causes the differences in the light absorption efficiency estimated from $a^*(440)$. However, the relationship between cell ESD and $a^*(440)$ was positive (i.e. the opposite of the expected relationship between cell size and light absorption efficiency). Therefore, it appears that cell size did not contribute to the observed variability in $a^*(440)$. In contrast, chl *a*:POC and $a^*(440)$ were negatively correlated ($r = -0.87$, $p < 0.01$) as expected if lower chl *a* cell content lessened the packaging effect. The increase in internal chl *a* content and the consequent reduction of $a^*(\lambda)$ in response to increasing nutrient concentration has been widely described in laboratory experiments performed with both diatoms and dinoflagellates (Reynolds et al. 1997, Stramski et al. 2002, Stæhr & Cullen 2003). Similarly, Mercado et al. (2008b) reported higher $a^*(440)$ values in natural communities of the Alboran Sea growing at nitrate limitation in comparison with non-limited communities. Consequently, the higher light absorption efficiency in the offshore communities fits the expected acclimation response to low nutrients. However, it cannot be discounted that the distinguishable taxonomic composition of the offshore communities contributed to their higher $a^*(440)$ since the chl *a* content per carbon unit in dinoflagellates is per se low in comparison with diatoms and other phytoplankton groups (Tang 1996). Furthermore, the larger cells have a greater ability to build vacuoles (Raven 1995), which decreases the chl *a* content per cell volume (Raven 1995).

It should be expected that these changes in light absorption efficiency do not affect the photosynthetic capacity of communities growing under non-limiting irradiance conditions (P_{max}). Consequently, the differences in biomass-specific carbon uptake rates ($VDIC$) among the surface communities of the coastal and offshore stations (which photosynthesize under non-limiting light) should be attributed to differences in Calvin cycle activity rather than to photoacclimation. Our data show that the coastal surface communities dominated by <50 µm diatoms had higher carbon uptake rates than the offshore communities dominated by dinoflagellates. Changes in P_{max} coinciding with increases in the contribution of dinoflagellates to phytoplankton biomass in natural communities have been previously described (Côté & Platt 1983, Shaw & Purdie 2001). Published data indicate that dinoflagellates have lower photosynthesis rates per carbon unit (Chan 1980) and higher metabolic costs in comparison with diatoms (Smayda 1997), which has been attributed to their lower chl *a* per carbon unit (Tang 1996). Therefore, the differences between coastal and offshore communities adequately fit the distinctive physiological performances of both groups. Dominance of dinoflagellates over diatoms at offshore stations could be explained by their capacity for adopting an alternative strategy to autotrophy for nutrient acquisition, as some of the species found in our samples have mixotrophic nutrition (e.g. *Prorocentrum minimum* and *Karenia brevis*; Li et al. 1996, Stoecker et al. 1997, Glibert et al. 2009). If that is the case, the inorganic nutrient uptake rates obtained in our study for the offshore communities could not reflect their actual nutrient acquisition rates. Li et al. (2012) found that mixotrophy in dinoflagellates could be a competition strategy during nutrient limitation.

Overall, the results demonstrate that acclimation strategies and physiological features of the dominant groups modulate the usage of light and nutrients by the community. These changes appear to depend weakly on the size-constraints (at least at the community level). Our results do not fully support the expected relationship between cell size and photosynthetic capacity (Stolte & Riegman 1995, Lohrenz et al. 2003, Irwin et al. 2006, Litchman et al. 2009, Key et al. 2010), at least when the features of the community as a whole are examined. Similarly, Huete-Ortega et al. (2011) reported that phytoplankton carbon fixation rates and cell size are often not correlated. Previously, several authors demonstrated that the slope of the size-scaling function of the phytoplankton metabolic rate is far from the expected value (the so called 3/4 rule; Dodds et al. 2001, Isaac & Carbone 2010) and Finkel et al. (2010)

obtained a slope much closer to 1 than 3/4 for the relationship between the specific growth rate as a function of cell size. Huete-Ortega et al. (2011) attributed the deviation of metabolic rates, predicted from their cell size and those actually measured, to the acquisition of taxa-specific physiological strategies by species belonging to a certain size class. Our data support this hypothesis and emphasize the necessity of considering the acclimation capacity of the communities to predict their role in carbon budgets.

Acknowledgements. This research was funded by National Secretariat of Research, Development and Innovation of the Spanish Government by means of the grants NITROALBORAN (CTM2006-00426) and TROFOALBORAN (CTM2009-07776/MAR) and co-funded by the EU. I.S. was supported by a studentship of the Education Ministry. We thank the crew of the RV 'García del Cid' for their invaluable help during the cruise.

LITERATURE CITED

Agawin N, Agustí S, Duarte CM (2002) Abundance of Antarctic picophytoplankton and their response to light and nutrient manipulation. Aquat Microb Ecol 29:161–172

Arín L, Morán XAG, Estrada M (2002) Phytoplankton size distribution and growth rates in the Alboran Sea (SW Mediterranean): short term variability related to mesoscale hydrodynamics. J Plankton Res 24:1019–1033

Armbrust EV, Chisholm SV (1992) Patterns of cell-size change in a marine centric diatom. Variability evolving from clonal isolates. J Phycol 28:146–156

Armstrong RA (2003) Representing biogeochemical diversity and size spectra in ecosystem models of the ocean carbon cycle. In: Canham CD, Cole J, Laurenroth WK (eds) Models in ecosystem science. Princeton University Press, Princeton, NJ, p 254–271

Azam F, Fenchel T, Field JG, Gray JS, Meyer-Reil LA, Thingstad F (1983) The ecological role of water-column microbes in the sea. Mar Ecol Prog Ser 10:257–263

Chan AT (1980) Comparative physiological study of marine diatoms and dinoflagellates in relation to irradiance and cell size. II. Relationship between photosynthesis, growth and carbon/chlorophyll *a* ratio. J Phycol 16: 428–432

Ciotti AM, Bricaud A (2006) Retrievals of a size parameter for phytoplankton and spectral light absorption by colored detrital matter from water-leaving radiances at SeaWiFS channels in a continental shelf region off Brazil. Limnol Oceanogr Methods 4:237–253

Ciotti AM, Lewis MR, Cullen JJ (2002) Assessment of the relationships between dominant cell size in natural phytoplankton communities and the spectral shape of the absorption coefficient. Limnol Oceanogr 47:404–417

Claustre H, Kerherve P, Marty JC, Prieur L, Videau C, Hecq JH (1994) Phytoplankton dynamics associated with a geostrophic front: ecological and biogeochemical implications. J Mar Res 52:711–742

Cleveland JS, Weidemann AD (1993) Quantifying absorption by aquatic particles: a multiple scattering correction for glass-fiber filters. Limnol Oceanogr 38:1321–1327

Côté B, Platt T (1983) Day-to-day variations in the spring summer photosynthetic parameters of coastal marine phytoplankton. Limnol Oceanogr 28:320–344

Dafner EV, Boscolo R, Bryden HL (2003) The N:Si:P molar ratio in the Strait of Gibraltar. Geophys Res Lett 30:1506, doi:10.1029/2002GL016274

Dodds PS, Rothman DH, Weitz JS (2001) Re-examination of the '3/4-law' of metabolism. J Theor Biol 209:9–27

Dugdale RC, Goering JJ (1967) Nutrient limitation in the sea: dynamics, identification, and significance. Limnol Oceanogr 12:685–695

Dugdale RC, Wilkerson FP (1986) The use of ^{15}N to measure nitrogen uptake in eutrophic oceans: experimental considerations. Limnol Oceanogr 31:673–689

Edwards FE, Thomas MK, Klausmeier CA, Litchman E (2012) Allometric scaling and taxonomic variation in nutrient utilization traits and maximum growth rate of phytoplankton. Limnol Oceanogr 57:554–566

Finkel ZV (2001) Light absorption and size scaling of light-limited metabolism in marine diatoms. Limnol Oceanogr 46:86–94

Finkel ZV, Beardall J, Flynn KJ, Quigg A, Rees TAV, Raven JA (2010) Phytoplankton in a changing world: cell size and elemental stoichiometry. J Plankton Res 32:119–137

Geider RJ, Platt T, Raven JA (1986) Size dependence of growth and photosynthesis in diatoms: a synthesis. Mar Ecol Prog Ser 30:93–104

Glibert PM, Burkholder JM, Kana TM, Alexander J, Skelton H, Shilling C (2009) Grazing by *Karenia brevis* on *Synechococcus* enhances its growth rate and may help to sustain blooms. Aquat Microb Ecol 55:17–30

Goldman JC (1993) Potential role of large oceanic diatoms in new primary production. Deep-Sea Res I 40:159–168

Gutiérrez-Rodríguez A, Latasa M, Agustí S, Duarte CM (2011) Distribution and contribution of major phytoplankton groups to carbon cycling across contrasting conditions of the subtropical northeast Atlantic Ocean. Deep-Sea Res I 58:1115–1129

Harrison W, Wood LJE (1988) Inorganic nitrogen uptake by marine picoplankton: evidence for size partitioning. Limnol Oceanogr 33:468–475

Hoepffner N, Sathyendranath S (1991) Effect of pigment composition on absorption properties of phytoplankton. Mar Ecol Prog Ser 73:11–23

Huete-Ortega M, Cermeño P, Calvo-Díaz A, Marañón E (2011) Isometric size-scaling of metabolism rate and the size abundante distribution of phytoplankton. Proc R Soc Lond B Biol Sci 279:1815–1823

Irigoien X, Flynn KJ, Harris RP (2005) Phytoplankton blooms: a 'loophole' in microzooplankton grazing impact? J Plankton Res 27:313–321

Irwin AJ, Finkel ZV, Schofield OME, Falkowski PG (2006) Scaling-up from nutrient physiology to the size-structure of phytoplankton communities. J Plankton Res 28: 459–471

Isaac NJB, Carbone C (2010) Why are metabolic scaling exponents so controversial? Quantifying variance and testing hypothesis. Ecol Lett 13:728–735

Jacquet S, Prieur L, Nival P, Vaulot D (2010) Structure and variability of the microbial community associated to the Alboran Sea frontal system (Western Mediterranean) in winter. J Oceanogr Res Dat 3:47–75

Kana TM, Glibert PM (1987) Effect of irradiance of up to 2000 µE m^{-2} s^{-1} on marine *Synechococcus* WH7803. 1. Growth, pigmentation and cell composition. Deep-Sea Res A 34:479–495

Kanda J, Laws EA, Saino T, Hattori A (1987) An evaluation of isotope dilution from conventional data sets of ^{15}N uptake experiments. J Plankton Res 9:79–90

Kara AB, Rochford PA, Hulburt HE (2000) Efficient and accurate bulk parameterizations of air-sea fluxes for use in general circulation models. J Atmos Ocean Technol 17:1421–1438

Key T, McCarthy A, Campbell DA, Six C (2010) Cell size trade-offs govern light exploitation strategies in marine phytoplankton. Environ Microbiol 12:95–104

Knap A, Michaels A, Close H, Ducklow H, Dickson A (1996) Protocols for the Joint Global Ocean Flux Study (JGOFS) core measurements. JGOFS Report No. 19, Reprint of the IOC manuals and guides, No. 29, UNESCO, Paris

Lafuente JG, Cano N, Vargas M, Rubín JP, Hernández-Guerra A (1998) Evolution of the Alboran Sea hydrographic structures during July 1993. Deep-Sea Res I 45:39–65

Li AS, Stoecker DK, Coats DW, Adam EJ (1996) Ingestion of fluorescently labeled and phycoerythrin-containing prey by mixotrophic dinoflagellates. Aquat Microb Ecol 10: 139–147

Li J, Glibert PM, Alexander JA, Molina ME (2012) Growth and competition of several harmful dinoflagellates under different nutrient and light conditions. Harmful Algae 13:112–125

Litchman E, Klausmeier CA, Yoshiyama K (2009) Contrasting size evolution in marine and freshwater diatoms. Proc Natl Acad Sci USA 106:2665–2670

Lohrenz S, Weidemann AD, Fuel M (2003) Phytoplankton spectral absorption as influenced by community size structure and pigment composition. J Plankton Res 25: 35–61

MacIsaac JJ, Dugdale RC (1972) Interactions of light and inorganic nitrogen in controlling nitrogen uptake in the sea. Deep-Sea Res 19:209–232

Menden-Deuer S, Lessard EJ (2000) Carbon to volume relationships for dinoflagellates, diatoms and other protist plankton. Limnol Oceanogr 45:569–579

Mercado JM, Ramírez T, Cortés D, Sebastián M, Vargas M (2005) Temporal changes of the phytoplankton communities in an upwelling area of the Alborán Sea. Sci Mar 69:451–465

Mercado JM, Cortés D, García A, Ramírez T (2007) Seasonal and inter-annual changes in the planktonic communities of the northwest Alboran Sea (Mediterranean Sea). Prog Oceanogr 74:273–293

Mercado JM, Ramírez T, Cortés D, Sebastián M, Liger E, Bautista B (2008a) Partitioning the effects of changes in nitrate availability and phytoplankton community structure on relative nitrate uptake. Mar Ecol Prog Ser 359: 51–68

Mercado JM, Ramírez T, Cortés D (2008b) Changes in nutrient concentration induced by hydrological variability and its effect on light absorption by phytoplankton in the Alborán Sea (Western Mediterranean Sea). J Mar Syst 71:31–45

Mercado JM, Sallés S, Cortés D (2011) Marine diatom communities: taxonomic variability, physiological plasticity and role in the carbon cycling at coastal upwelling areas. In: Compton JC (ed) Diatoms: ecology and life cycle. Nova Publishers, Hauppauge, NY, p 37–62

Mercado JM, Cortés D, Ramírez T, Gómez F (2012) Hydrological forcing masks the potential impact of nutrient release from diffuse sources in the NW coast of the Alboran Sea. Hydrobiologia 680:91–107

Millard RC, Owens WB, Fofonoff NP (1990) On the calculation of the Brunt-Väisälä frequency. Deep-Sea Res A 37:167–181

Minas HJ, Coste B, LeCorre P, Minas M, Raimbault P (1991) Biological and geochemical signatures associated with the water circulation through the Strait of Gibraltar and in western Alboran Sea. J Geophys Res 96:8755–8771

Morán XAG, Estrada M (2001) Short-term variability of photosynthetic parameters and particulate and dissolved primary production in the Alboran Sea (SW Mediterranean). Mar Ecol Prog Ser 212:53–67

Morel A, Ahn YH, Partensky F, Vaulot D, Claustre H (1993) *Prochlorococcus* and *Synechococcus*: a comparative study of their optical properties in relation to their size and pigmentation. J Mar Res 51:617–649

Morin PJ, Fox JW (2004) Diversity in the deep blue sea. Nature 429:813–814

Nogueira E, González-Nuevo G, Bode A, Varela M, Morán XAG, Valdés L (2004) Comparison of biomass and size spectra derived from optical plankton counter data and net samples: application to the assessment of mesoplankton distribution along the Northwest and North Iberian Shelf. ICES J Mar Sci 61:508–517

Olenina I, Hajdu S, Edler L, Andersson A and others (2006) Biovolumes and size-classes of phytoplankton in the Baltic Sea. HELCOM Balt Sea Environ Proc 106:1–144

Parrilla G, Kinder TH (1987) Oceanografía física del Mar de Alborán. Bol Inst Esp Oceanogr 4:133–165

Ramírez T, Cortés D, Mercado JM, Vargas-Yañez M, Sebastián M, Liger E (2005) Seasonal dynamics of inorganic nutrients and phytoplankton biomass in the NW Alboran Sea. Estuar Coast Shelf Sci 65:654–670

Raven JA (1995) Scaling the seas. Plant Cell Environ 18: 1090–1100

Raven JA, Kübler JE (2002) New light on the scaling of metabolic rate with the size of algae. J Phycol 38:11–16

Reul A, Rodríguez V, Jiménez-Gómez F, Blanco JM and others (2005) Variability in the spatio-temporal distribution and size-structure of phytoplankton across an upwelling area in the NW-Alboran Sea (W-Mediterranean). Cont Shelf Res 25:589–608

Reynolds R, Stramski D, Kiefer DA (1997) The effect of nitrogen limitation on the absorption and scattering properties of the marine diatom *Thalasiossira pseudonana*. Limnol Oceanogr 42:881–892

Ribes M, Coma R, Gili JM (1999) Seasonal variation of particulate organic carbon, dissolved organic carbon and the contribution of microbial communities to the live particulate organic carbon in a shallow near-bottom ecosystem in the Northwestern Mediterranean Sea. J Plankton Res 21:1077–1100

Rodríguez J (1994) Some comments on the size-based structural analysis of the pelagic ecosystem. Sci Mar 58: 1–10

Rodríguez V, Blanco JM, Jiménez-Gómez F, Rodríguez J, Echevarría F, Guerrero F (1997) Distribución espacial de algunos estimadores de biomasa fitoplanctónica y material orgánico particulado en el mar de Alborán, en condiciones de estratificación térmica (julio de 1993). Publ Espec Inst Esp Oceanogr 24:53–64

Rodríguez J, Blanco JM, Jiménez-Gómez F, Echevarría F and others (1998) Patterns in the size structure of the phytoplankton community in the deep fluorescence maximum of the Alboran Sea (southwestern Mediterranean). Deep-Sea Res I 45:1577–1593

Rodríguez J, Tintoré J, Allen JT, Blanco JM and others (2001) Mesoscale vertical motion and the size structure of phytoplankton in the ocean. Nature 410:360–363

Sarhan T, García-LaLafuente J, Vargas M, Vargas JM, Plaza P (2000) Upwelling mechanisms in the northwestern Alborán Sea. J Mar Syst 23:317–331

Savenkoff C, Chanut JP, Vezina AF, Gratton Y (1995) Distribution of biological-activity in the lower St. Lawrence estuary as determined by multivariate analysis. Estuar Coast Shelf Sci 40:647–664

Shaw PJ, Purdie DA (2001) Phytoplankton photosynthesis-irradiance parameters in the near-shore UK coastal waters of the North Sea: temporal variation and environmental control. Mar Ecol Prog Ser 216:83–94

Silovic T, Ljubesic Z, Mihanovic H, Olujic G, Terzic S, Jaksic Z, Vilicic D (2011) Picoplankton composition related to thermohaline circulation: the Albanian boundary zone (southern Adriatic) in late spring. Estuar Coast Shelf Sci 91:519–525

Smayda TJ (1997) Harmful algal blooms: their ecophysiology and general relevance to phytoplankton blooms in the sea. Limnol Oceanogr 42(5, Part 2):1137–1153

Stæhr P, Cullen JJ (2003) Detection of *Karenia mikimotoi* by spectral absorption signatures. J Plankton Res 25: 1237–1249

Stoecker DK, Li A, Coats DW, Gustafson DE, Nannen MK (1997) Mixotrophy in the dinoflagellate *Prorocentrum minimum*. Mar Ecol Prog Ser 152:1–12

Stolte W, Riegman R (1995) Effect of phytoplankton cell size on transient-state nitrate and ammonium uptake kinetics. Microbiology 141:1221–1229

Stramski D, Sciandra A, Claustre H (2002) Effects of temperature, nitrogen, and light limitation on the optical properties of the marine diatom *Thalassiosira pseudonana*. Limnol Oceanogr 47:392–403

Sun J, Liu D (2003) Geometric models for calculating cell biovolume and surface area for phytoplankton. J Plankton Res 25:1331–1346

Sverdrup HU (1953) On conditions for the vernal blooming of phytoplankton. J Cons Int Explor Mer 18:287–295

Tang EPY (1996) Why do dinoflagellates have lower growth rates? J Phycol 32:80–84

Thompson PA, Guo MX, Harrison PJ (1992) Effects of variation in temperature. I. On the biochemical composition of 8 species of marine phytoplankton. J Phycol 38: 1347–1364

Tintoré J, Gomis D, Alonso S, Parrilla G (1991) Mesoscale dynamics and vertical motion in the Alboran Sea. J Phys Oceanogr 21:811–823

Tomas CR (1997) Identifying marine phytoplankton. Academic Press, London

Tremblay JE, Legendre L, Therriault JC (1997) Size-differential effects of vertical stability on the biomass and production of phytoplankton in a large estuarine system. Estuar Coast Shelf Sci 45:415–431

Trüper HG, Yentsch CS (1967) Use of glass-fiber filters for the rapid preparation of *in vivo* absorption spectra of photosynthetic bacteria. J Bacteriol 94:1255–1256

Utermöhl H (1958) Zur Vervollkommnung der quantitativen Phytoplankton-Methodik. Mitt Int Ver Theor Angew Limnol 9:1–38

Vadrucci MR, Cabrini M, Basset A (2007) Biovolume determination of phytoplankton guilds in transitional water ecosystems of Mediterranean Ecoregion. Transit Waters Bull 2:83–102

Vaulot D, Courties C, Partensky F (1989) A simple method to preserve oceanic phytoplankton for flow cytometric analysis. Cytometry 10:629–635

Verity P, Robertson CY, Tronzo CR, Andrews MG, Nelson JR, Sieracki ME (1992) Relationship between cell volume and carbon and nitrogen content of marine photosynthetic nanoplankton. Limnol Oceanogr 37:1434–1446

Editorial responsibility: Katherine Richardson, Copenhagen, Denmark

Submitted: April 25, 2013; Accepted: October 25, 2013
Proofs received from author(s): February 7, 2014